In: CARDIOVASCULAR SYSTEMS DYNAMICS Ed. J.Baan,A.Noordergraaf,J.Rain
MIT Press, Cambridge Mass. 1978

21

Interaction in the Microcirculation

HARVEY N. MAYROVITZ,
MARY P. WIEDEMAN, AND
ABRAHAM NOORDERGRAAF

INTRODUCTION

An array of interacting biological processes affect and/or control the hemodynamic and exchange characteristics of the microcirculation. Microvessel diameter modulation, both precapillary (vasomotion) and postcapillary (venomotion), is one such process and is the focus of interest in this paper. Though dynamic aspects of vasomotion and venomotion have been demonstrated [1, 2], neither the separate nor the interactive effects are adequately understood. Microvessel dimensional [3, 4] and hemodynamic [5, 6] measurements have recently provided limited data of sufficient reliability to be useful in this context. Undoubtedly, as the present substantial technical problems are overcome, additional pertinent information will emerge. However, because of the extreme complexity of the microvasculature, the important problem of structuring and interpreting these data in a way that provides new insight into the integrated behavior of the microcirculation needs to be dealt with. Toward this end, a quasi-static mathematical characterization of the microvasculature, using the bat wing as an experimental prototype, has recently been developed [7]. In the present paper this characterization will be extended to include precapillary sphincter dynamics, venomotion, and dynamic aspects of capillary exchange. It is our intent to develop this Microvascular Model and to examine its utility in extending our understanding of the way in which vascular dynamics influences hemodynamics and function within the microvasculature.

MODEL DEVELOPMENT

Model Configuration

Two major criteria guide the structuring of the model. First, it is necessary to characterize vasomotion and venomotion with detail and physiological properties sufficient to meet the primary objective of studying the separate and interactive effects at the microcirculatory level. Second, since each part of a microvascular region is affected by local conditions both upstream and downstream, and since these local conditions are affected by the macrocirculation, it is necessary to represent the microvascular region being studied in a way which includes its pertinent intrinsic characteristics and yet maintains the appropriate macroscopic properties of the total vascular bed.

The general form of a microvascular model which satisfies these structural requirements is shown in Figure 21.1. The purpose of the figure is to show the basic structure of the model and to serve as a guide for the description of the synthesis of the parts. The meaning and reasoning behind the inclusion of each part of the model follow.

The region bounded by the pressures P_0 and P_{10} represents a vascular unit from small artery through small vein. The part labeled "shunt pathway" is meant to account for the fact that there are many such pathways; it thus incorporates the effect of the multiple branches of the small artery. The resistance $R_i^{(SA)}$, seen looking into the point labeled P_0, has been previously computed and experimentally verified [7]. The input and output resistance distributions, represented by the quantities $R_i^{(a)}$, $R_0^{(SA)}$, and $R_0^{(a)}$, also correspond to previously determined quantities. The parts labeled

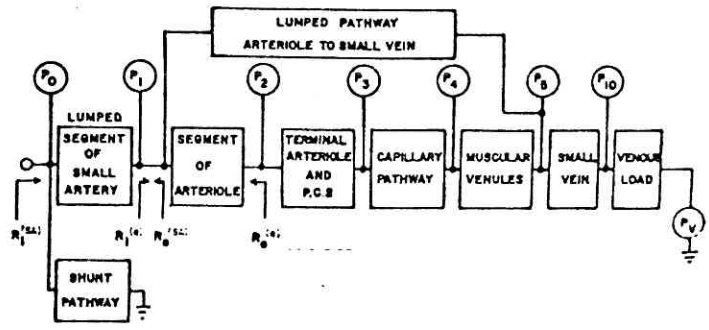

FIGURE 21.1 The general form of a microvascular model.
$R_1^{(SA)}$ is the equivalent input resistance "seen" looking into small artery from artery.
$R_1^{(a)}$ is the equivalent input resistance "seen" looking into arteriole from small artery.
$R_0^{(SA)}$ is the equivalent input resistance "seen" looking back into small artery from arteriole.
$R_0^{(a)}$ is the equivalent input resistance "seen" looking back into the arteriole supplying the capillary pathway.

"lumped segment of small artery" and "segment of arteriole" have values which, when combined with the remainder of the model, result in the input resistance calculated for the bed [7]. The part labeled "terminal arteriole and precapillary sphincter (PCS)" represents the dynamic properties of vasomotion and the hydraulic characteristics. The part labeled "capillary pathway" includes the filtration characteristics of the true capillaries and the hydraulic properties of the capillary and postcapillary venules. The part labeled "muscular venules" represents a lumped characterization of the distributed muscular venules. The part labeled "lumped pathway arteriole to small vein" represents the remainder of the arteriole–small vein pathways associated with the vascular unit. The part labeled "small vein" represents the dynamic and hydraulic characteristics of the rhythmically active postcapillary vessels. "Venous load" and P_V represent the impedance seen by the small veins and the central venous pressure.

The region P_1-P_2-P_3-P_4-P_5 represents the properties and behavior of the most basic subdivision of the microvascular field. Thus, capillary behavior is characterized in a setting where physiological pressures, flows, and impedances are obtained as a natural consequence of the interaction between pre- and postcapillary regions. In addition, in the pre- and postcapillary regions physiological conditions are also obtained, which permits the study of both local microvascular aspects and macrocirculatory interactions.

It now remains to develop the detailed mathematical representation of the component parts of the model. For this purpose electrical analogs provide a convenient method of visualizing the details of the microvasculature and their interrelationships, as well as a concise way of representing the defining mathematical equations. Such analogs are employed freely, but it should be emphasized that their physical construction is not intended. Rather, the equations which are embodied in the analogs are to be solved by computer.

Model of Rhythmically Active Postcapillary Vessels

Postcapillary vessels show as their most dominant characteristic a rhythmic variation in diameter. We must incorporate this active characteristic as well as the passive properties of these vessels into our model. To develop this portion of the model we start with a four-element passive electrical network to represent a general vessel segment (following Noordergraaf [8]), and then we modify this network to include aspects important for the active postcapillary vessel. The inductance of the four-element model, which represents fluid inertia, is small with respect to the viscous factors represented by series resistance and is therefore neglected. (This conclusion is based on examination of the prevailing Reynolds number of the small postcapillary vessels.) The shunt conductance of the four-element model represents leakage flow which leaves the vessel segment via branches. In the postcapillary vasculature flow enters at branch points and is handled as such. The active and time-varying characteristics of the vessels are accounted for by assigning time-varying properties to the resistance and compliance parameters.

Having arrived at a representation of a vessel segment, we now proceed to characterize a vessel of length and properties corresponding to those in the postcapillary vasculature.

Vessels are taken to be straight and cylindrical in shape. If we denote inside radius by a, wall thickness by h, and total length by l, then the resistance r and compliance c per unit length are given by

$$r = \frac{8\eta}{\pi a^4}, \tag{21.1}$$

$$c = \frac{3\pi a^2}{E} \frac{[(a/h) + 1]^2}{2(a/h) + 1}, \tag{21.2}$$

where η is the blood viscosity and E is the elastic modulus of the vessel wall. When r and c are multiplied by the segment length Δz, analog model parameters R and C are obtained.

To this point, the form of the segmental variation in the resistance and compliance has been left unspecified. As can be seen from Equations 21.1 and 21.2, both of these parameters depend on the vessel radius, while the compliance also depends on the ratio of radius to wall thickness and on the wall elastic modulus. To characterize the time-varying nature of these parameters, this mutual dependence on vessel radius must be taken into account. Further, since changes in vessel radius are associated with changes in the radius-to-wall-thickness ratio, the radius variation may not be chosen arbitrarily as a parameter forcing function. For the model to be realistic, we must therefore describe the vessel radius and wall-thickness variation in terms of the physical processes producing this variation.

Using the general characterization of vessel wall visoelastic properties developed by Westerhof and Noordergraaf [9], one can show that for the low-frequency, narrow-band case applicable to venomotion, a suitable approximation is given by

$$\sigma(t) = E\varepsilon(t) + K_\eta \dot{\varepsilon}(t), \tag{21.3}$$

where σ and ε are wall stress and strain, respectively, and the superior dot indicates differentiation with respect to time. Written in this form, Equation 21.3 is the

defining equation for the Voigt model of a vessel wall, with E and K_η being lumped elastic and viscous coefficients, respectively.

Utilization of Equation 21.3 requires the inclusion of muscle contraction effects in a way that accounts for vessel wall thickness. This requires in turn that an appropriate radius for these non-thin-walled vessels be defined, so that the strain terms of the equation can be interpreted unambiguously.

It may be shown that under conditions of equilibrium and subject to the normal range of intravascular pressure, the radius corresponding to a fully relaxed vessel state is ideally suited as such a reference radius [7]. Further, the effect of the contracting muscle may be taken into account by associating with the contraction process an additional force tending to reduce the vessel radius and thus disturb any quasi-equilibrium state assigned to the relaxed vessel. The inclusion of the influence of the contracting muscle is effected by expressing the left-hand side of Equation 21.3 as the difference between the stress tending to dilate the vessel and the developed stress σ_m associated with the contracting muscle. For a radius-to-wall-thickness ratio γ and inside and outside pressures P_i and P_o, respectively, the wall dynamics is described by

$$\gamma (P_i - P_o) - P_o - \sigma_m = E\varepsilon + K_\eta \dot{\varepsilon}. \tag{21.4}$$

The number of sections required to represent the vessel adequately depends on the physical length of each segment in relation to the smallest-wavelength disturbance present in the vessel. The predominant frequencies present (and those which represent the main source of periodic disturbance) lie in the band from 0.1 to 0.5 Hz.

Calculations of the wave velocities associated with these perturbations show that five segments are sufficient to represent small veins having mean lengths of 3–4 mm even when higher-order harmonics associated with nonsinusoidal perturbations are taken into account.

The vessel model at this point in its development is shown in Figure 21.2. Two additional features included to increase its generality are the potential for branch flow and nonuniform contraction of the rhythmically

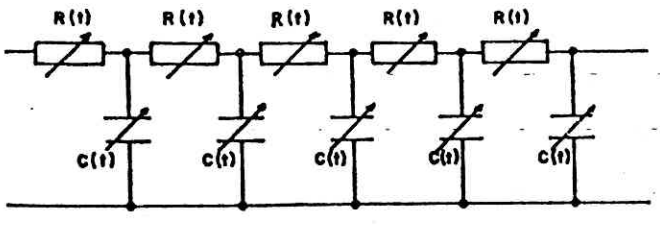

FIGURE 21.2 Representation of rhypthmically active vessel as five consecutive segments of time-varying resistance $R(t)$ and compliance $C(t)$.

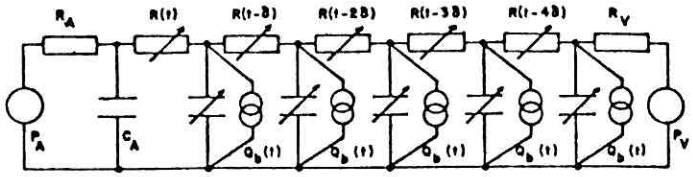

FIGURE 21.3 Representation of rhythmically varying vessel which includes branch flow $Q_b(t)$ and provision for temporal phase differences between contraction of spatially separated vessel regions (δ is the time delay between adjacent sections). Double circles symbolize branch flow sources.

active vessels. Experimental observations clearly indicate that following a contraction of the active vessel and the subsequent reduction in intravascular volume, there is a "filling" phase while the vessel relaxes [7]. The inflow during this period is due to a summation of inflows from individual branches. To include the essence of this effect, a flow source $Q_b(t)$ is associated with each segment, as illustrated in Figure 21.3. This representation allows us to study the effect of valves guarding the entrance of the branches to the small vein by setting the branch flow to be zero over part of the venomotion cycle, or to exclude it entirely by making it identically zero. For example, to model the situation in which the change in segmental volume accompanying venomotion is due to a modulation of the feeding branch flows, we set

$$Q_b(t) = 2\pi a \dot{a} \Delta z, \tag{21.5}$$

where Δz is the segment length. Then, to model the effect of the presence of the valves at the entrance regions, we would require that

$$Q_b(t) = \begin{cases} 2\pi a \dot{a} \Delta z & \text{for } \dot{a} \geq 0, \\ 0 & \text{for } \dot{a} < 0. \end{cases} \tag{21.6}$$

These relationships establish a pattern in which flow enters from the branches during the relaxation phase of venomotion and the inflow is stopped during the contraction phase. To exclude the branch flow entirely, $Q_b(t)$ is made zero.

The other feature incorporated into the model shown in Figure 21.3 is the provision for phase differences between contractions of spatially separated vessel regions. This feature is represented by associating with each segment's resistance and compliance a time delay δ. The inclusion of this nonuniform characteristic in the model permits evaluation of the significance of the peristaltic character sometimes associated with the rhythmic diameter variations seen in the postcapillary vessels. Since uniform vessel contraction is obtained by making the time delay zero, the model shown in Figure 21.3 is a most general representation.

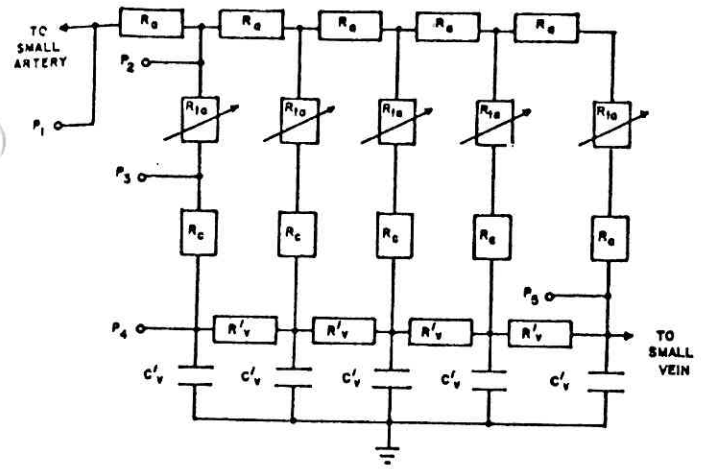

FIGURE 21.4 Vascular region from arteriole to muscular venule. R_a, R_{ta}, R_c, and R'_v represent segments of arteriole, terminal arteriole, capillary, and muscular venule, respectively. C'_v represents muscular venule compliance. P_1 through P_5 are the pressures shown in Figure 21.1.

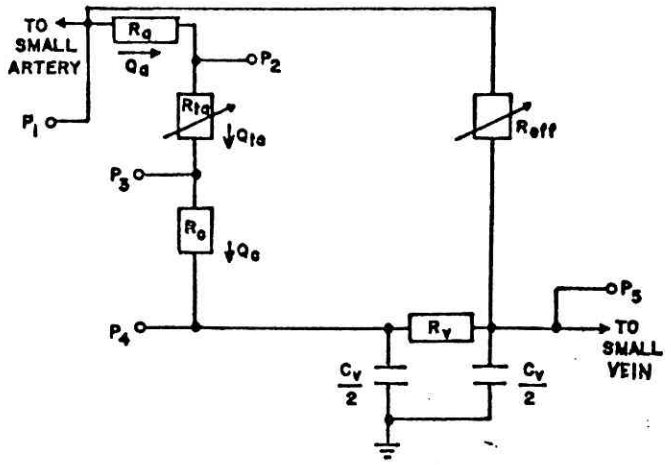

FIGURE 21.5 Reduced model of vascular region from arteriole to muscular venule. R_v and C_v are the lumped resistance and compliance of the muscular venule, respectively.

Model of Precapillary and Capillary Regions

In this section the region bounded by P_1 and P_5 in Figure 21.1 will be modeled. Figure 21.4 shows a detailed version of the vascular region from arteriole to muscular venule. The parts labeled R_a represent segments of the arteriole, R_{ta} represents the terminal arteriole and precapillary sphincter, and R_c represents the capillary region. The segmented RC network identified by R'_v and C'_v, into which the capillaries terminate, represents the muscular venule. The equations which characterize the hemodynamics in these vessels will be presented below. It is our present purpose to utilize Figure 21.4 as a reference to synthesize a reduced representation which will be coupled to the model of the rhythmically active vessel developed above. Our objective is to obtain a reduced version which contains the basic features of the more detailed version of Figure 21.4.

The first step is to lump the distributed venule which serves as the load for the capillary pathways and the source for the small vein. Next, because we are interested in isolating a single capillary pathway from the remainder of the network for detailed study, while maintaining the appropriate source impedance seen by the small veins, we have one of the pathways shown in Figure 21.4 enter this lumped venule at its origin and the remainder enter at the junction of the venule and the small vein. To account for the fact that the flow entering the small vein is due to the composite flow of the remaining arteriole pathways feeding that small vein, we represent these together with the four remaining pathways as a lumped pathway identified by R_{eff} in Figure 21.5. The quantity R_{eff} thus represents the effective flow resistance of all these pathways.

The flow regime in the arteriole segments is taken as obeying the Casson equation, and the flow regime in the terminal arteriole, capillary, and venule (subscripts ta, c, and v) is described by the following resistance functions:

$$R_{ta} = \frac{128\eta}{\pi} \frac{(2 - e^{-1.14/\nu_{ta}})}{D_{ta}^4} \times \frac{[1 + \frac{1}{4}\nu_{ta} + (\frac{1}{4}\nu_{ta})^4](1 + 0.6e^{-\beta_s})l_{ta}}{D_{ta}^4}, \quad (21.7)$$

$$R_c = \frac{128\eta}{\pi} \frac{(2 - e^{-1.14/\nu_c})}{D_c^4} \times \frac{[1 + \frac{1}{4}\nu_c + (\frac{1}{4}\nu_c)^4](1 + 0.6e^{-\beta_s})l_c}{D_c^4}, \quad (21.8)$$

$$R_v = \frac{128\eta}{\pi} \frac{(2 - e^{-1.14/\nu_v})}{D_v^4} \times \frac{[1 + \frac{1}{4}\nu_v + (\frac{1}{4}\nu_v)^4](1 + 0.6e^{-\beta_s})l_v}{D_v^4}, \quad (21.9)$$

where D is the vessel diameter, η is the plasma viscosity, ν is the ratio of undistorted red blood cell dimension to the inside diameter of the vessel, and β_s is the ratio of average red blood cell separation to vessel diameter.

Inclusion of Precapillary Sphincter Activity

In Figures 21.4 and 21.5 the quantity R_{ta} is shown with an arrow through it. This representation calls attention to the fact that because of the vasomotion associated with this microvascular region, the resistance is a dynamic function. This aspect is included implicitly in Equation 21.7 by representing vasomotion as a controlled variation of D_{ta} and ν_{ta}. Thus, all we need do is represent these quantities as appropriate time functions. However, the physiological question of which microvascular factor is the dominant controller of sphincter activity has yet to be resolved. Theories concerning sphincter control

may be grouped into two rather broad categories: direct mechanical effects controlling sphincter activity, and metabolic control. Mechanical effects would encompass the myogenic theory, which maintains that contraction is stimulated by elevation in intravascular pressure, and the tissue pressure theory, which maintains that sphincter activity can be explained on the basis of diameter-induced changes due to direct coupling of the tissue pressure to the vessel. The second category includes the array of chemicals and other vasoactive substances whose concentrations vary as a function of the local metabolic state of the tissue.

In the present model precapillary sphincter activity is controlled in such a fashion as to maintain (within physiological limits) the tissue pressure in the dependent microvascular regions. There are several reasons for this type of characterization. First, from the limited amount of experimental data available, the normal tissue pressure appears to be maintained within narrow limits. This does not necessarily imply that such maintenance is caused by sphincter activity, but it does offer that possibility. Second, use of an extravascular quantity (tissue pressure) rather than an intravascular one (capillary pressure) permits the controlled quantity to reflect more closely the local tissue environment which, in the final analysis, must be the ultimate controlled variable. Third, by using tissue pressure we in effect include the myogenic theory as a special case. For example, if osmotic quantities are held constant in the model, the resultant sphincter activity should be similar to that associated with the maintenance of the capillary pressure. It should be emphasized that at this point no postulation or speculation is made concerning the mechanism of sphincter control, except that its activity is such as to maintain the tissue pressure within specified limits.

To accomplish this mathematically, the terminal arteriole is taken to have a maximum (D_r) and minimum (D_c) inside diameter corresponding to those observed in vivo. If we denote the upper and lower tissue pressure limits as P_{tu} and P_{tl}, the terminal arteriole diameter D_{ta} and lumen-to-red-cell ratio ν_{ta} in Equation 21.7 are parametrically controlled by the tissue pressure according to

$$\begin{aligned} D_{ta} &= D_c \quad \text{for} \quad P_t \geq P_{tu}, \\ D_{ta} &= D_r \quad \text{for} \quad P_t \leq P_{tl}, \\ D_{ta} &= D_c + m_1 t \quad \text{for} \quad P_{tl} < P_t < P_{tu} \text{ (dilation phase)}, \\ D_{ta} &= D_r - m_2 t \quad \text{for} \quad P_{tl} < P_t \leq P_{tu} \text{ (contraction phase)}, \end{aligned} \tag{21.10}$$

where m is the rate of change of the vessel diameter.

Inclusion of Capillary Filtration

Classically, considerations of capillary filtration have been approached by describing filtration and reabsorption through steady-state fluid-balance equations.

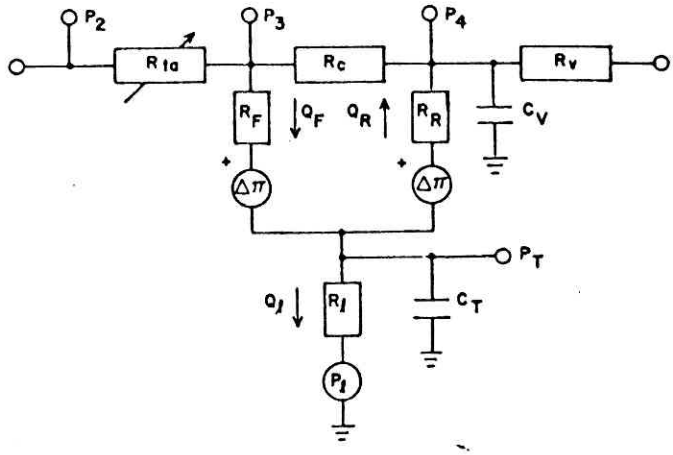

FIGURE 21.6 Inclusion of capillary filtration. Flows Q_F, Q_R, and Q_I represent filtration, reabsorption, and lymph flow, respectively. P_I is a pressure source representing the pressure in the lymph vessels, and $\Delta\pi$ is a pressure source representing the effective intravascular-extravascular osmotic pressure difference. P_3 and P_4 are the pressures that would be measured at the arterial and venous side of the capillary, respectively. R_F and R_R represent the effective resistance to filtration and reabsorption and are related to the filtration and reabsorption coefficients.

Figure 21.6 shows the model representation of a filtration-reabsorption process. It includes both steady-state and dynamic relationships and, in addition, takes into account the effects of lymph flow and the compliance of the perivascular space (C_T). These aspects are important (especially the compliance) when the dynamic character of the fluid-exchange process is to be taken into account. The model equations for this region are listed below.

In Figure 21.6, R_{ta} and venous compliance and resistance, which are not part of the filtration model per se, are shown in order to call attention to the fact that capillary hemodynamics and hence the fluid-exchange process are not steady-state phenomena. Thus, it should be expected that the protein concentration in the extravascular space will vary with intravascular dynamics. Since the osmotic pressure difference depends on this concentration, it may be concluded that the parameter $\Delta\pi$ in the model of Figure 21.6 is subject to parametric variation. The precise form of this parametric variation is unknown. Most experiments which have attempted to examine the dynamic character have done so under conditions of zero lymph flow. We take this condition as the starting point in an attempt to characterize the time dependence of this process.

Let $\Delta\pi_0$ represent the equilibrium osmotic pressure difference defined for the condition $Q_F = Q_R$ and $Q_I =$

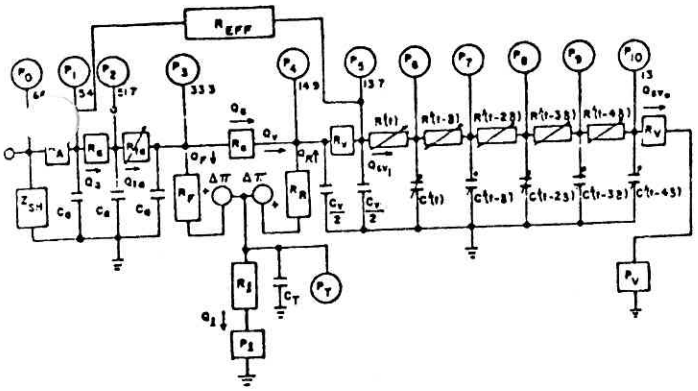

FIGURE 21.7 The detailed microvascular model. Parameters are defined in Table 21.1. Numbers adjacent to pressure symbols (circles) are the measured pressures at these points (in mm Hg).

0, where Q_F, Q_R, and Q_l represent filtration, reabsorption, and lymph flow, respectively. Under these conditions there is a corresponding equilibrium tissue volume (V_0) and pressure (P_{T0}). A perturbation in intravascular pressure must then be accompanied by a change in $\Delta\pi$ away from its equilibrium value. This change may be taken as proportional to the change in tissue fluid volume. Mathematically, this leads to

$$\Delta\pi = \Delta\pi_0 + K_\pi C_T (P_T - P_{T0}), \tag{21.11}$$

relating the osmotic pressure difference $\Delta\pi$ to the reference value $\Delta\pi_0$ and the deviation of the tissue pressure from a corresponding reference. This will be used as an approximation to describe the parametric variation in osmotic pressure difference associated with intravascular induced alterations in tissue pressure.

Composite Microvascular Model and Computer Evaluation

Figure 21.7 displays the detailed microvascular model obtained when the model of the rhythmically active vessel is coupled to the precapillary and capillary models. The figure has the same form as the general model shown in Figure 21.1, but it now includes a detailed representation of the individual parts. For the reader's convenience, the parameters used in the model with their definitions are listed in Table 21.1.

The equations which mathematically describe the Microvascular Model shown in Figure 21.7 are as follows:

$$\dot{P}_1 = \frac{P_0 - P_1}{C_a R_A} - \frac{P_1 - P_2}{C_a R_a}, \tag{21.12}$$

$$\dot{P}_2 = \frac{P_1 - P_2}{C_a R_a} - \frac{P_2 - P_3}{C_a R_{ta}} - \frac{P_2 - P_5}{C_a R_{EFF}}, \tag{21.13}$$

TABLE 21.1
Symbols and definitions used in the microvascular model of Figure 21.7

Symbol	Definition
C_a	Lumped compliance associated with the arterial vessels
$C'(t)$	Compliance of a segment of the rhythmically active vessel
C_T	Effective compliance of the tissue space
C_v	Lumped compliance of the distributed muscular venules
P_l	Pressure in the lymph vessels
$P_i (i = 0, 1, \ldots, 10)$	Pressures within the vasculature
P_T	Tissue pressure
P_V	Central venous pressure
$Q_b(t)$	Branch inflow to the rhythmically active vessel
R_a	Effective resistance of the arteriole vessels
R_A	Effective resistance associated with the small artery
$R'(t)$	Resistance of a segment of the rhythmically active vessel
R_l	Flow resistance to lymph from the interstitial space to the lymph capillaries
R_C	Flow resistance of the true capillary and the postcapillary venule
R_{EFF}	Lumped pathway for the remainder of the arteriole-to-small-vein pathways
R_F	Effective resistance associated with fluid filtration from the capillary into the interstitial space (reciprocal of the filtration coefficient)
R_R	Effective resistance associated with fluid reabsorption from the interstitial space (reciprocal of the reabsorption coefficient)
R_{ta}	Flow resistance associated with the terminal arteriole and precapillary sphincter
R_v	Lumped resistance of the muscular venule
R_V	Equivalent resistance seen by the rhythmically active vessel looking toward the large veins
Z_{SH}	Impedance associated with the remaining branches of the small artery
δ	Time delay associated with the variation in $R'(t)$ and $C'(t)$ between axially separated segments
$\Delta\pi$	The difference between the osmotic pressure in the capillary and the interstitial space

$$\dot{P}_3 = \frac{P_2 - P_3}{C_a R_{ta}} - \frac{P_3 - P_4}{C_a R_C} - \frac{P_3 - P_T - \Delta\pi}{C_a R_F}, \quad (21.14)$$

$$\dot{P}_T = \frac{P_3 - P_T - \Delta\pi}{C_v R_F} - \frac{P_T - R_L}{C_T R_L} - \frac{P_T + \Delta\pi - P_4}{C_T R_R}, \quad (21.15)$$

$$\dot{P}_4 = \frac{2(P_3 - P_4)}{C_v R_C} + \frac{2(P_T + \Delta\pi - P_4)}{C_v R_R} - \frac{2(P_4 - P_5)}{C_v R_v}, \quad (21.16)$$

$$\dot{P}_5 = \frac{2(P_4 - P_5)}{C_v R_v} + \frac{2(P_2 - P_5)}{C_v R_{EFF}} - \frac{2(P_5 - P_6)}{C_v R'(t)}, \quad (21.17)$$

$$\dot{P}_6 = \frac{P_5 - P_6}{C'(t)R'(t)} - \frac{P_6 - P_7}{C'(t)R'(t-\delta)} + \frac{Q_b(t)}{C'(t)} - \frac{P_6\dot{C}'(t)}{C'(t)}, \quad (21.18)$$

$$\dot{P}_7 = \frac{P_6 - P_7}{C'(t-\delta)R'(t-\delta)} - \frac{P_7 - P_8}{C'(t-\delta)R'(t-2\delta)} + \frac{Q_b(t-\delta)}{C'(t-\delta)} - \frac{P_7\dot{C}'(t-\delta)}{C'(t-\delta)}, \quad (21.19)$$

$$\dot{P}_8 = \frac{P_7 - P_8}{C'(t-2\delta)R'(t-2\delta)} - \frac{P_8 - P_9}{C'(t-2\delta)R'(t-3\delta)} + \frac{Q_b(t-2\delta)}{C'(t-2\delta)} - \frac{P_8\dot{C}'(t-2\delta)}{C'(t-2\delta)}, \quad (21.20)$$

$$\dot{P}_9 = \frac{P_8 - P_9}{C'(t-3\delta)R'(t-3\delta)} - \frac{P_9 - P_{10}}{C'(t-3\delta)R'(t-4\delta)} + \frac{Q_b(t-3\delta)}{C'(t-3\delta)} - \frac{P_9\dot{C}'(t-3\delta)}{C'(t-3\delta)}, \quad (21.21)$$

$$\dot{P}_{10} = \frac{P_9 - P_{10}}{C'(t-4\delta)R'(t-4\delta)} - \frac{P_{10} - P_v}{C'(t-4\delta)R_v} + \frac{Q_b(t-4\delta)}{C'(t-4\delta)} - \frac{P_{10}\dot{C}'(t-4\delta)}{C'(t-4\delta)}. \quad (21.22)$$

The equations for the resistance $R'(t)$ and compliance $C'(t)$ associated with the rhythmically active vessel are given by Equations 21.1 and 21.2, respectively, after multiplication by the segment length. The radius and radius-to-wall-thickness variation, which determine the time properties of these parameters, are given as the solutions to Equation 21.3. The branch flow $Q_b(t)$ is given by Equation 21.6. The functions which mathematically characterize the resistances R_C of the capillary region and R_v of the muscular venule region are given by Equations 21.8 and 21.9, respectively. The function that characterizes the resistance R_{ta} associated with the terminal arteriole and precapillary sphincter is given by Equation 21.7, subject to the parametric variation defined by Equation 21.10. The remaining resistance and compliance functions are of the form given by Equations 21.1 and 21.2 using the appropriate dimensional quantities. Finally, the parametric variation in the osmotic pressure difference is determined by Equation 21.11.

Solution of Equations

The pressures and flows in the Microvascular Model of Figure 21.7, given by Equations 21.12–21.22, are variables which are dependent on the parameter values of the model. Some of these parameters are, in turn, dependent on the values of the pressures and flows, so that the system is inherently nonlinear. In order to represent adequately and to analyze the dynamic activity of the rhythmically active vessel, the precapillary sphincter activity, the parametric control, and the mutual interaction of these with the hemodynamic variables, it is necessary to have a solution method which accounts for this nonlinearity. In the present case a hybrid computer solution was utilized to solve Equations 21.12–21.22.

RESULTS

We present in this section results which illustrate some of the basic effects of the separate and composite actions of vasomotion and venomotion.

Venomotion

As described previously, the left-hand side of Equation 21.4 represents the difference between the wall stress tending to cause the vessel to dilate and the active stress tending to cause it to contract. For convenience, we call the net stress tending to dilate the vessel the "effective wall stress" (S_e). In the results to be presented, the effective stress is the driving function responsible for the resultant parameter variation. In Figure 21.8 the onset of muscle contraction is shown as a reduction in S_e since an increase in muscle contraction reduces the effective stress tending to dilate the vessel. In the example shown in this figure, the contraction phase lasts for one second, at which time the force developed by the muscle decreases to its basal tone level in a linear fashion and at a rate slower than that at which it developed the force.

The time relationship between the simulated muscle contraction, the resultant effective wall stress, and the effect on internal radius a, wall thickness h, segmental resistance R, and segmental compliance C are illustrated in Figure 21.8A. Muscle contraction initiates a reduction in internal radius and a simultaneous increase in vessel wall thickness. The immediate consequence is an increase in segmental resistance and a decrease in compliance. When relaxation occurs, all parameters return toward their resting levels.

The effects of these parameter changes on pressure

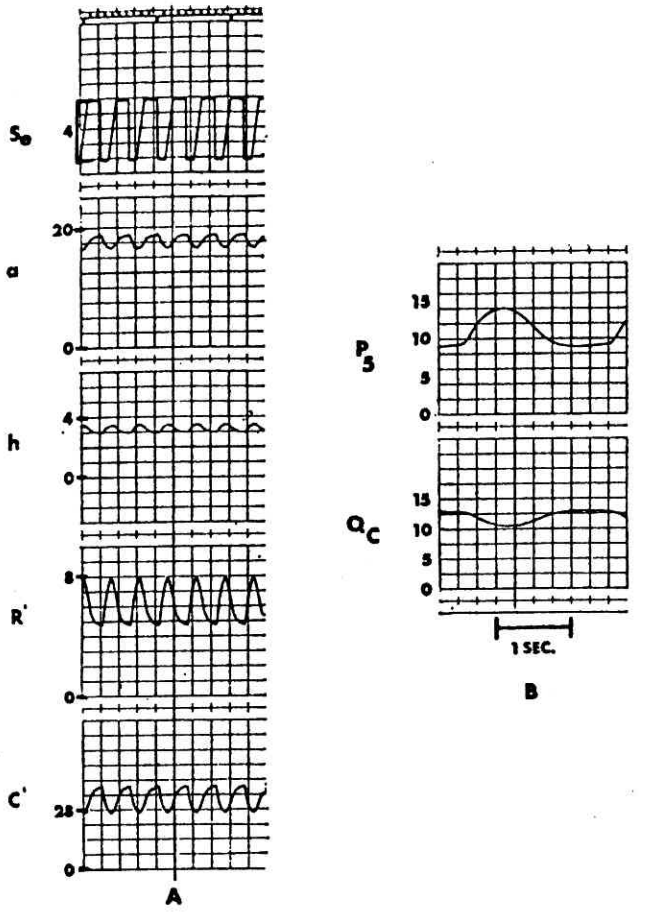

FIGURE 21.8 Parameter variation and hemodynamics accompanying venomotion. A: The time variation of vessel radius a, wall thickness h, segmental resistance R', and segmental compliance C' associated with an effective muscle contraction S_e. Units: a and h in microns; R' in 10^8 dyne sec cm^{-5}; C' in 10–12 $dyne^{-1}$ cm^5; and S_e in 10^5 dyne cm^{-2}. Time marks at top represent 1 sec intervals. B: Pressure and capillary flow. Units: P_5 in mm Hg and Q_C in 10^{-9} cm^3/sec.

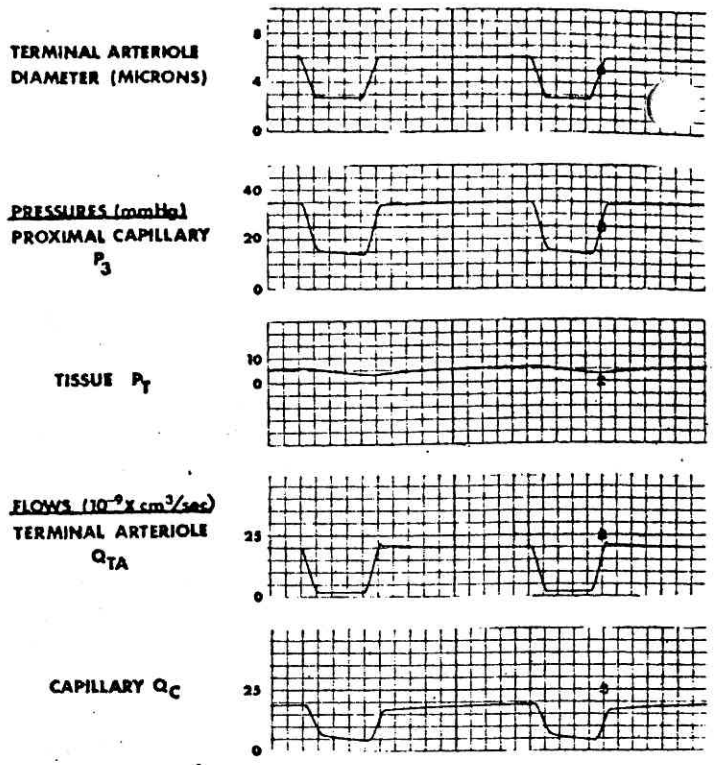

FIGURE 21.9 Hemodynamics associated with terminal arteriole vasomotion. Quantities shown are those corresponding to the Microvascular Model. Major divisions represent 2 sec intervals.

and flow are shown in Figure 21.8B. The postcapillary vessel pressure rises rapidly by about 5 mm Hg due to contraction and returns to its baseline value at a considerably slower rate. Concomitant with this elevation in postcapillary pressure is a reduction in capillary flow.

Arteriole Vasomotion

The arteriole vasomotion associated with local control is caused by diameter variation of the distal segment of the terminal arteriole. This diameter variation is associated with a time variation of the effective resistance in the terminal arteriole pathway, which depends, in its turn, on the instantaneous vessel diameter. The hemodynamic consequences of this activity are illustrated in Figure 21.9.

Reduction in terminal arteriole diameter produces a precipitous fall in capillary pressure. This pressure drop is associated with a decrease in tissue pressure which continues until the terminal arteriole begins to dilate. The flow through the arteriole is similarly reduced by the contraction. A significant point to note is the relationship between this flow (i.e., the capillary inflow) and the outflow of the capillary. When the terminal arteriole is dilated, the capillary outflow is less than the inflow by an amount equal to the net filtration flow. When the arteriole contracts, both flows decrease, but the capillary outflow is larger than the terminal arteriole flow. This is due to the increase in fluid reabsorption (with respect to filtration) associated with the decrease in intravascular pressure. Thus, one clear consequence of the arteriole (or precapillary sphincter) vasomotion is the production of a dynamic mode of capillary filtration and reabsorption.

Vasomotion and Venomotion

Figure 21.10 illustrates the combined effect of venomotion and terminal arteriole and precapillary sphincter vasomotion on pressure and capillary flow. The results shown are for uniform contraction at three different venomotion frequencies. The large rise in capillary flow is associated with the dilation phase of vasomo((sphincter opening). Superimposed on this flow change is a smaller and higher-frequency fluctuation due to

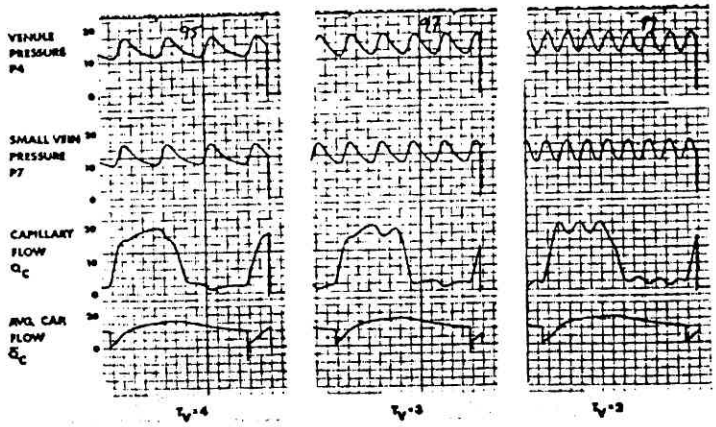

FIGURE 21.10 Combined effect of venomotion and vasomotion on capillary flow. T_V is the fundamental period of venomotion in seconds, pressure is in mm Hg, flows in units of 10^{-9} cm³/sec, time marks at 1 sec intervals.

venomotion. For each of the venomotion frequencies shown, the capillary flow component due to venomotion is larger when the sphincters are fully open. Thus, for example, at a venomotion frequency of 0.5 Hz the peak-to-peak capillary flow modulation produced by venomotion is 4×10^{-9} cm³ sec^{-1} when the sphincter is open and 2.5×10^{-9} cm³ sec^{-1} when the sphincter is at its minimum diameter. However, if the venomotion contribution is expressed as a percent of the maximum flow, we find that when the sphincter is in its contracted state, the modulation in capillary flow due to venomotion is 50%.

From these results, then, it would appear that under normal conditions and with the sphincters fully dilated, the capillary flow is determined mainly by precapillary dynamics. With decreasing terminal arteriole diameter the modulation in capillary flow is determined principally by postcapillary dynamics.

In Figure 21.11 the effect of arteriolar pressure variation on sphincter dynamics as predicted by the model is compared with available experimental data. In the bottom part of the figure the ratio of contraction duration to vasomotion period derived from the model is plotted as a function of perfusion pressure for venous pressures of 5 and 10 mm Hg (dashed and solid lines, respectively). Superimposed (filled circles) is the data of Wiedeman [2], obtained by observing the terminal arteriole contraction duration in response to elevated arterial pressure. The experimental data fit the characteristics predicted by the model. In addition, the model predicts that elevation of venous pressure will result in an increase in the contraction fraction of the precapillary sphincter—a hypothesis not yet confirmed by experiment.

In the upper part of the figure the capillary flow associated with vasomotion is illustrated. The value at

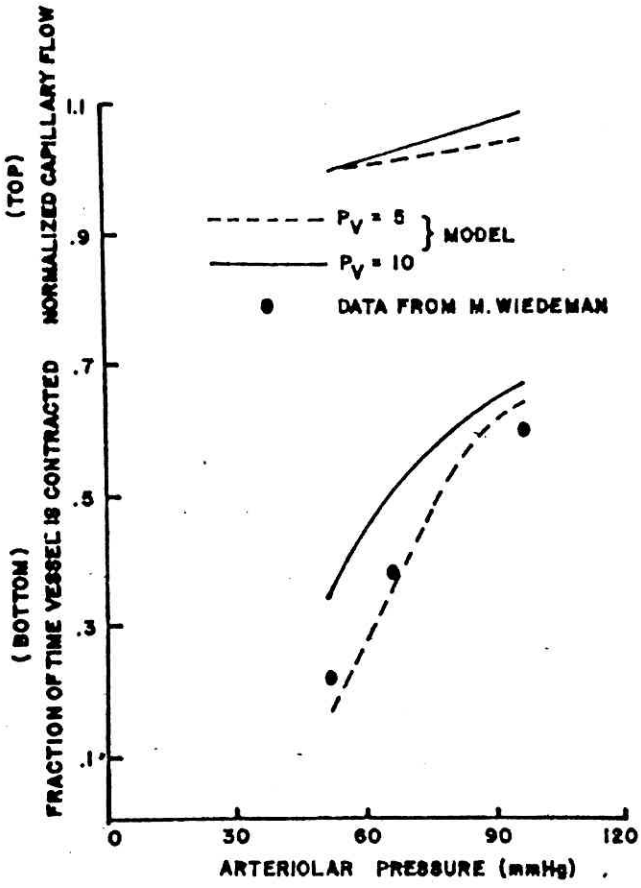

FIGURE 21.11 Contraction duration and capillary flow dependence on arteriolar pressure.

70 mm Hg, which is taken as the control perfusion pressure, is normalized to unity. The results indicate that one consequence of the vasomotion dynamics is an effective autoregulation of capillary flow.

DISCUSSION

Using a microvascular model and pertinent experimental data, we have attempted to clarify and quantify the hemodynamic and functional significance and interaction of dynamic processes in the precapillary (vasomotion), capillary (filtration), and postcapillary (venomotion) vascular regions.

The spontaneous diameter changes associated with the terminal arterioles and precapillary sphincters (vasomotion) produce a modulation of the pressure and flow in the capillary networks. This modulation has several effects. The decrease in diameter is associated with a drop in pressure at the arterial end of the capillary by an amount which depends on the amount of diameter change. For the diameter changes most frequently observed experimentally, the capillary pressure is reduced from a value of about 40 mm Hg to a value close

to the venous pressure (10–15 mm Hg). This means that the contraction phase of vasomotion reduces capillary pressure to a value below the commonly accepted normal value of plasma osmotic pressure (25 mm Hg). This implies that the contraction phase of vasomotion is associated with capillary reabsorption over the entire capillary length for normal arterial pressures.

Thus, the classical picture of a rather steady filtration on the arterial side of the capillary and reabsorption on the venous side does not appear applicable on two counts. First, the process is anything but steady since the capillary dynamics has an almost random quality. Second, confinement of the filtration-reabsorption process to anatomic positions of the capillary does not conform to the predicted hydrodynamic pressures required for these events to occur.

It was further shown that increasing the arterial pressure in the Microvascular Model resulted in a nonlinear increase in the amount of time the precapillary sphincters were closed. Comparison with in vivo data obtained in the bat wing showed excellent quantitative agreement. In addition, the model results showed that this mode of control simultaneously produced an autoregulation of the average capillary flow.

Study of the postcapillary microvasculature has yielded evidence indicating that, in addition to the precapillary dynamics, the rhythmic diameter variation of the muscular venules and small veins (termed venomotion) plays a significant role in determining the flow and pressure distribution in the microcirculation. Though the fundamental mechanisms controlling venomotion have not yet been fully elucidated, the responses of these postcapillary vessels to pressure perturbations and the presence of substantial vascular smooth muscle in the walls of these vessels clearly suggest that there is a substantial myogenic component involved. The persistence of venomotion in the denervated preparation [10] further supports the idea of a local mechanism associated with active contraction. Whether the myogenic response is stimulated by pressure per se, or by vessel distention, is not clear. However, detailed examination of the characteristic properties of venomotion has shown that elevations in frequency secondary to pressure elevation stimuli are produced by an increase in the rate of distention, with no significant change in the time course of the contraction phase [6]. This contraction is associated with an increase in segmental vascular resistance and vessel wall thickness and a decrease in vascular compliance. The contraction causes the instantaneous pressure within these vessels to rise by an amount which depends on the absolute value of the venous pressure existing prior to the contraction and on the strength of contraction; the pressure rise ranges from 6 to 10 mm Hg. These values represent a significant increase in the venule and small vein pressure in view of the normal mean pressure levels in these postcapillary vessels (10–15 mm Hg). The pressure elevations due to contraction predicted by the model are consistent with measured values in the bat wing [11].

The amount of control exercised by postcapillary dynamics depends on the state of the precapillary sphincter supplying the dependent capillary region.

The most dramatic effects on capillary flow are related to alterations in the precapillary sphincter state. However, when the sphincter is in its contracted state, the modulation in capillary flow due to venomotion (expressed as a percentage of the maximum capillary flow associated with that sphincter state) may be 50% or larger.

It appears that under normal conditions the significance of venomotion for capillary flow modulation waxes and wanes with alternate contraction and dilation phases of vasomotion. From this it follows that increases in relative contraction time of the sphincter would assign to the postcapillary vasculature and associated dynamics an increasingly significant role as determinants of capillary flow distribution and as factors in venous circulation. One may speculate, then, that physiological conditions which tend to augment the constrictor phase of vasomotion will simultaneously increase both the local and systemic importance of the postcapillary vasculature.

Systemic hypertension is a pathological condition which, according to the present results, should augment the constrictor phase of vasomotion. This implies that vascular and cellular changes accompanying or following hypertension are, to a large extent, dependent on the functional capacity and integrity of the postcapillary microvasculature. In contrast, systemic hypotension due to hemorrhage or myocardial infarction would tend to increase the dilation phase and reduce the dynamic component of vasomotion. This reduction represents the diminution of a control component to which the capillary and postcapillary microvasculature are sensitive. The so-called state of irreversibility of shock may, therefore, be associated with the expected decrease in venomotion accompanying the loss of sufficient dynamic or triggering input from the precapillary vasculature. The new concepts which have evolved from the present work regarding the pre- and postcapillary interaction, the pressure-dependent control range of vasomotion, and the dynamic aspects of capillary exchange should pave the way for a deeper insight into the vascular aspects of these pathological conditions. In addition, the overall Microvascular Model and conceptual framework of the microcirculation should provide a basis for extending

our understanding of numerous aspects of vascular function and microvascular hemodyamics in both health and disease.

ACKNOWLEDGMENT

HNM's research is supported by U.S. Public Health Service Grant SCOR, Thrombosis HL14217. AN's research is supported by USPHS Grant HL 10330.

REFERENCES

1. Nicoll, P. A., and Webb, R. L. 1955. Vascular patterns and active vasomotion as determiners of flow through minute vessels. *Angiology* 6: 291–310.
2. Wiedeman, M. P. 1966. Contractile activity of arterioles in the bat wing during intraluminal pressure changes. *Circ. Res.* 19: 559–563.
3. Wiedeman, M. P. 1963. Dimensions of blood vessels from distributing artery to collecting vein. *Circ. Res.* 12: 375–381.
4. Intaglietta, M., and Zweifach, B. W. 1971. Geometrical model of the microvasculature of rabbit omentum from in vivo measurements. *Circ. Res.* 28: 593–600.
5. Wiederhielm, C. A., and Weston, B. V. 1973. Microvascular, lymphatic, and tissue pressures in the unanesthetized mammal. *Am. J. Physiol.* 225: 992–996.
6. Mayrovitz, H. N. 1977. Microvascular blood velocities measured in the unanesthetized mammal. *Am. J. Physiol.* (in press).
7. Mayrovitz, H. N. 1974. The microcirculation: Theory and experiment. Unpublished Ph.D. dissertation, University of Pennsylvania.
8. Noordergraaf, A. 1966. Development of an analog computer for the human systemic arterial system. In A. Noordergraaf, G. N. Jager, and N. Westerhof, eds., *Circulatory Analog Computers* (Amsterdam: North Holland Publishers).
9. Westerhof, N., and Noordergraaf, A. 1971. Arterial viscoelasticity: A generalized model. *J. Biomech.* 3: 357.
10. Wiedeman, M. P. 1968. Blood flow through terminal arterial vessels after denervation of the bat wing. *Circ. Res.* 22: 83.
11. Wiederhielm, C. A. 1969. The interstitial space and lymphatic pressures in the bat wing. In A. P. Fishman, ed., *The Pulmonary Circulation and Interstitial Space* (Chicago: University of Chicago Press), pp. 29–40.

DISCUSSION

DR. MELBIN: I am still trying to formulate this, Harvey, so I'll ramble just a bit. The statement you made was that in hypertension you apparently will have the increased arterial constriction and the capillary bed will take on more of the venous characteristics. Did I understand that correctly?

DR. MAYROVITZ: That was roughly it, yes.

DR. MELBIN: I am thinking of the Starling Law phenomenon in terms of hydrostatic pressure and transmission of fluid into the interstitium, which leads me into a reverse situation; that is, the hypertension then should reduce the outward passage of fluid because the capillary beds are at lower pressures, should it not?

DR. MAYROVITZ: Elevation of arterial pressure up here is one thing. It's another thing to say what it is at the capillary. Are you suggesting that arterial pressure measured at a macroscopic vessel will of necessity reflect a similar change at the capillary?

DR. MELBIN: I wasn't thinking so much of central pressure. I am trying to relate to your model of peripheral vasoconstriction, the arterial vasoconstriction and the capillary beds—that is, vessels that occur after that constriction and that take on the venous characteristic, which means that it should upset the transfer of fluid by other than diffusive mechanisms into the interstitium. Do you think that this is a logical sequence?

DR. MAYROVITZ: It may be, but it does depend on the pressure in the capillary, which may or may not drop—you don't really know, do you? You've got vasoconstriction at some level. The amount by which that will reduce the capillary pressure depends on how much it is elevated at the macroscopic level as well as on what is happening on the venule side. If indeed capillary pressure dropped, as you indicated, then you would expect exactly what you say.